JGR Oceans

RESEARCH ARTICLE
10.1029/2019JC015125

Key Points:
- The remote sensing reflectance (R_{rs}) in a virtual 412-nm band can be estimated for Landsat 8
- The estimation of R_{rs}(412) allows to semianalytically derive the absorption coefficients of water components from Landsat 8 reflectance
- The phytoplankton, CDOM, and detritus absorption coefficients derived from simulated Landsat 8 data are satisfactorily accurate

Correspondence to:
J. Wei,
jianwei.wei@umb.edu

Citation:
Wei, J., Lee, Z. P., Shang, S., & Yu, X. (2019). Semianalytical derivation of phytoplankton, CDOM, and detritus absorption coefficients from the Landsat 8/OLI reflectance in coastal waters. *Journal of Geophysical Research: Oceans*, *124*. https://doi.org/10.1029/2019JC015125

Received 5 MAR 2019
Accepted 1 MAY 2019
Accepted article online 7 MAY 2019

Semianalytical Derivation of Phytoplankton, CDOM, and Detritus Absorption Coefficients From the Landsat 8/OLI Reflectance in Coastal Waters

Jianwei Wei[1], ZhongPing Lee[1], Shaoling Shang[2], and Xiaolong Yu[1]

[1]School for the Environment, University of Massachusetts Boston, Boston, MA, USA, [2]State Key Laboratory of Marine Environmental Science, Xiamen University, Xiamen, Fujian, China

Abstract The Operational Land Imager (OLI) onboard Landsat 8 has potential for mapping the water bio-optical properties with high spatial resolution. Landsat 8/OLI generates the remote sensing reflectance (R_{rs}) at four visible bands ($\lambda_{1\text{-}4}$ = 443, 482, 561, and 655 nm) and is lack of a 412-nm band commonly included for ocean color sensors. This spectral configuration has limited the use of Landsat 8/OLI reflectance product for analytical derivation of light absorption coefficients of phytoplankton, colored dissolved organic matter (CDOM), and detritus. In this study, we proposed a hybrid approach to fill this gap. First, we developed an algorithm to estimate the reflectance in a virtual band centered at λ_0 = 412 nm from the OLI reflectance spectra $R_{rs}(\lambda_{1\text{-}4})$. Both the estimated $R_{rs}(\lambda_0)$ and measured $R_{rs}(\lambda_{1\text{-}4})$ were then used together to retrieve the water component absorption coefficients with existing algorithms including the quasi-analytical algorithm. We assessed the model performance using in situ measurements from the global waters. It was found that the proposed approach could estimate R_{rs}(412) with a median absolute percentage difference of ~9%. The subsequent retrievals of the component absorption coefficients were satisfactorily accurate, with median absolute percentage difference roughly equal to 35%, 40%, and 60% for phytoplankton, CDOM, and detritus, respectively. The results suggest the feasibility to generate analytically the component absorption coefficients from the Landsat 8/OLI reflectance.

1. Introduction

Phytoplankton, colored dissolved organic matter (CDOM), and detritus are important components of coastal aquatic ecosystems. Phytoplankton harvest spectral radiation to convert inorganic carbon to organic carbon through photosynthesis (Morel, 1991), which sustains the aquatic food web. CDOM and detritus absorb light strongly in the ultraviolet and blue bands, protecting living organisms from damaging radiation (Bricaud et al., 1981). Monitoring the variability of phytoplankton, CDOM, and detritus light absorption coefficients (denoted as a_{ph}, a_g and a_d, respectively) is thus crucial for understanding the status of ecological systems, carbon cycles, and water quality related problems (Hansell & Carlson, 2001; Kim et al., 2016; Yu et al., 2016).

Satellite remote sensing represents a unique avenue for synoptic and frequent observation of the global waters. The water color instruments such as the Moderate Resolution Imaging Spectroradiometer and the Visible and Infrared Spectroradiometer can provide the remote sensing reflectance (R_{rs}, sr^{-1}) at multiple bands centered around 412, 443, 488, 550, and 670 nm. These multiband R_{rs} data have been extensively used to estimate the phytoplankton, CDOM, and detritus absorption coefficients in various types of waters (Binding et al., 2008; Cao & Miller, 2015; Ciotti & Bricaud, 2006; Mannino et al., 2014; Siegel et al., 2005). However, these satellite data are typical of coarse spatial resolutions (~1 km), insufficient for observation of the bio-optical variability in the dynamic nearshore environments. Landsat 8 satellite is a new member of the land remote sensor family. To the interests of the aquatic science community, the Operational Land Imager (OLI) onboard measures R_{rs} with a spatial resolution of ~30 m and with much enhanced radiometric performance at four visible bands ($\lambda_{1\text{-}4}$, centered at 443, 482, 561, and 655 nm; Markham et al., 2014). Recent studies show that the OLI reflectance product over waters can be acceptable after atmospheric correction (Pahlevan et al., 2017; Wei et al., 2018). Over the last few years, the OLI observation has quickly found its applications in various aquatic studies. In particular, many empirical methods were used for the estimation of the CDOM absorption coefficient (Alcântara et al., 2016; Olmanson et al., 2016;

Snyder et al., 2017) and phytoplankton chlorophyll a concentration (CHL, milligram per cubic meter; Kim et al., 2016; Lee et al., 2019; Snyder et al., 2017). Still, there exists no operational semianalytical (SA) procedures specific to the OLI data for the derivation of the absorption coefficients from active components, such as phytoplankton. Considering the potential and readiness of the high-resolution satellite observation, it is highly necessary to explore analytical approaches to facilitate the processing and application of the OLI data.

Many SA algorithms exist and can be used to retrieve the absorption coefficient of phytoplankton and the absorption coefficient due to the colored detrital matters (CDM; including CDOM and detritus; denoted as a_{dg}) from multiband R_{rs} spectra (Brando et al., 2012; Carder et al., 1999; Hoge & Lyon, 1996; Lee et al., 1998; Lee et al., 2002; Maritorena et al., 2002; Werdell et al., 2013; Werdell et al., 2018). And almost all the SA algorithms require the $R_{rs}(412)$ data in their procedures, because the reflectance at this blue band provides great constraints for robust partition of phytoplankton and CDM (Carder et al., 1991; Wei et al., 2016). For instance, the quasi-analytical algorithm (QAA; Lee et al., 2002) is a stepwise procedure to determine the particle backscattering coefficient (b_b) and bulk or total absorption coefficient (a), which explicitly uses R_{rs} measurements at 412 nm to partition a_{ph} and a_{dg}. The spectral optimization algorithms also specifically use $R_{rs}(412)$ in their procedures (Maritorena et al., 2002; Werdell et al., 2013). The Landsat 8/OLI is lack of a 412-nm band, thus has no $R_{rs}(412)$ measurement. It is challenging to directly apply the existing SA algorithms to the OLI reflectance data for the retrieval of component absorption coefficients.

In this study, we propose a hybrid approach for systematic derivation of the component absorption coefficients from Landsat 8 reflectance data. This approach uses an existing Semi-Analytical algorithm with a Virtual-band Estimator (SAVE). The virtual-band estimator estimates the remote sensing reflectance in a virtual band centered at 412 nm (designated as λ_0) for an OLI reflectance spectrum $R_{rs}(\lambda_{1\text{-}4})$. Then $R_{rs}(\lambda_0)$ and $R_{rs}(\lambda_{1\text{-}4})$ are combined into a new spectrum, $R_{rs}(\lambda_{0\text{-}4})$, which is further used to derive a, a_{ph}, and a_{dg} products from the QAA algorithm. Last, the a_{dg} product is partitioned into a_d and a_g with an empirical algorithm. The retrievals are validated with in situ measurements from the global waters, which shows promising performance (section 4). As a convenient approach, we recommend the use of SAVE to generate the absorption coefficients of water components from the Landsat 8/OLI reflectance data.

2. Algorithm Development and Configuration

2.1. Lookup Table for R_{rs} Spectral Shapes

To estimate $R_{rs}(412)$ from the OLI $R_{rs}(\lambda_{1\text{-}4})$ data, a lookup table (LUT) for the R_{rs} spectral shapes centered at $\lambda_{0\text{-}4}$ was created from two hyperspectral R_{rs} data sets. The first set of data were in situ measurements (400-800 nm with 3-nm increment) collected from the global waters; a detailed description can be found in Wei et al. (2016). The second data set was simulated with the Hydrolight radiative transfer simulation software (version 5.1; Mobley & Sundman, 2008). For the simulation, we adopted the inherent optical property (IOP) data including the absorption spectra of phytoplankton, detritus, and CDOM and the backscattering spectra of phytoplankton and detritus (b_{bph} and b_{bd}) from International Ocean Color Coordinating Group (IOCCG, 2006), with the following modifications. First, we assumed the Fournier-Forand phase function for particle scattering for every model runs, with a constant particle backscattering ratio $\tilde{b}_{bp} = 0.013$ (Whitmire et al., 2007). The pure water absorption coefficient and scattering coefficient were adopted from Lee et al. (2015) and Zhang et al. (2009), respectively. The inelastic scattering was also included in the simulation with default configurations (Mobley & Sundman, 2008), where the chlorophyll fluorescent quantum efficiency was set to 0.02, the CDOM fluorescence was modeled using the spectral fluorescence quantum efficiency function of Mobley (1994), and the Raman scattering cross-section was set to 2.6×10^{-4} m^{-1} at the reference wavelength of 488 nm. Two solar zenith angles (30° and 60°) under clear sky were considered for mild sea states (wind speed $w_s = 5$ m/s). The simulation resulted in 1,000 hyperspectral R_{rs} spectra (400-800 nm with 5-nm increment). Collectively, the field data and the synthetic R_{rs} data represent a wide range of waters with CHL varying from ~0.03 to >50 mg/m^3.

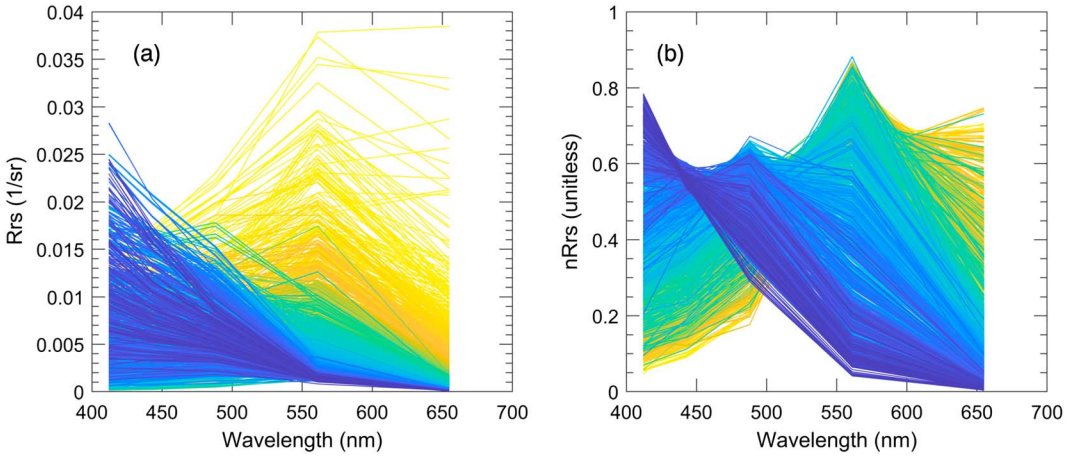

Figure 1. (a) Remote sensing reflectance spectra at five bands $\lambda_{0\text{-}4}$ = 412, 443, 482, 561, and 655 nm. (b) The lookup table of normalized remote sensing reflectance. As described in the text, $R_{rs}(\lambda_{1\text{-}4})$ spectra are convolved to Landsat 8/OLI bandwidths.

In the second step, the in situ and simulated hyperspectral R_{rs} spectra were convolved to OLI's bands $\lambda_{1\text{-}4}$ through

$$R_{rs}(\lambda_i) = \frac{\int_{400}^{800} R_{rs}(\lambda) RSR^i d\lambda}{\int_{400}^{800} RSR^i d\lambda}, \mathrm{i} = 1, 2, 3, \text{and } 4, \tag{1}$$

where RSR^i is the acronym for OLI's relative spectral responsivity for band λ_i. This step is necessary since OLI has wide bandwidths with full width at half maximum of 15, 60, 57, and 37 nm at 443, 482, 561, and 655 nm, respectively. In addition, the hyperspectral R_{rs} data were interpolated at 412 nm to obtain $R_{rs}(\lambda_0)$. Here we assumed that the virtual band λ_0 has a narrow bandwidth of 5 nm and hence no spectral weighting was applied to it. The derived five-band R_{rs} spectra are presented in Figure 1a.

Each individual five-band R_{rs} spectrum was then normalized by the root of the sum of squares (RSS) of R_{rs} values from λ_0 to λ_4 as in Wei, Lee, and Shang (2016),

$$nR_{rs}^*(\lambda_i) = \frac{R_{rs}(\lambda_i)}{\left[\sum_{j=0}^{4} R_{rs}(\lambda_j)^2\right]^{1/2}}, \mathrm{i} = 0, 1, 2, 3 \text{ and } 4, \tag{2}$$

where nR_{rs}^* is the normalized R_{rs} spectrum. All such normalized spectra are further illustrated in Figure 1b. From the definition of normalization in equation (2), the $nR_{rs}^*(\lambda_{0\text{-}4})$ spectra are characteristic of unique features. First, the band ratios of $nR_{rs}^*(\lambda_{0\text{-}4})$ remain the same with corresponding $R_{rs}(\lambda_{0\text{-}4})$. Second, the spectral curvature remains unchanged. Third, the magnitudes of nR_{rs}^* vary from zero to one, inclusively. Last, the RSS of $nR_{rs}^*(\lambda_{0\text{-}4})$ is always equal to one. These $nR_{rs}^*(\lambda_{0\text{-}4})$ spectra will be used to represent the R_{rs} spectral shapes occurring in natural waters perceived by OLI.

2.2. Virtual-Band Estimator

With a given Landsat 8/OLI $R_{rs}(\lambda_{1\text{-}4})$ spectrum, the virtual-band estimator first seeks to identify an $nR_{rs}^*(\lambda_{0\text{-}4})$ spectrum from the LUT, which has the closest spectral shape to $R_{rs}(\lambda_{1\text{-}4})$. To do so, we calculate the cosine distance between $R_{rs}(\lambda_{1\text{-}4})$ and every $nR_{rs}{}^*$ spectra in the LUT as

$$d = 1 - \frac{\sum_{i=1}^{4} \left[nR_{rs}^*(\lambda_i) \cdot R_{rs}(\lambda_i)\right]}{\sqrt{\sum_{i=1}^{4} \left[nR_{rs}^*(\lambda_i)\right]^2 \sum_{i=1}^{4} \left[R_{rs}(\lambda_i)\right]^2}}, \tag{3}$$

where d is the distance formed by the two vectors of $nR_{rs}^*(\lambda_{1\text{-}4})$ and $R_{rs}(\lambda_{1\text{-}4})$. The nR_{rs}^* spectrum with the minimum cosine distance to $R_{rs}(\lambda_{1\text{-}4})$ will be determined and chosen for subsequent application.

It is assumed that the "new" spectrum $R_{rs}(\lambda_{0\text{-}4})$, composed of known $R_{rs}(\lambda_{1\text{-}4})$ and an estimated $R_{rs}(\lambda_0)$, has the spectral shape that best represents the reflectance spectrum of the targeted water. Following equation (2), we normalized the R_{rs} spectrum at 412 nm and further let it be equal to $nR^*_{rs}(412)$,

$$\frac{R_{rs}(\lambda_0)}{\left[R_{rs}(\lambda_0)^2+\sum_{i=1}^{4}R_{rs}(\lambda_i)^2\right]^{1/2}}\approx nR^*_{rs}(412), \tag{4}$$

where the denominator in the left-hand side of equation (4) refers to the RSS of $R_{rs}(\lambda_{0\text{-}4})$, while the right-hand side is the value extracted from the above-selected nR^*_{rs} spectrum. With only one unknown, equation (4) can be solved for $R_{rs}(\lambda_0)$ as

$$R_{rs}(\lambda_0)=A\times nR^*_{rs}(412), \tag{5}$$

where A is a scaling factor with

$$A=\left[\sum_{i=1}^{4}\left(R_{rs}(\lambda_i)\right)^2\right]^{1/2}\Big/\left[\sum_{k=1}^{4}\left(nR^*_{rs}(\lambda_k)\right)^2\right]^{1/2}. \tag{6}$$

With the above estimated $R_{rs}(\lambda_0)$ and known $R_{rs}(\lambda_{1\text{-}4})$, the new $R_{rs}(\lambda_{0\text{-}4})$ spectrum will be used for the derivation of light absorption coefficients of water components in a procedure described below.

2.3. Inversion of Inherent Optical Properties

We adopted the QAA algorithm of Lee et al. (2002) for the IOP inversion from $R_{rs}(\lambda_{0\text{-}4})$. The original QAA algorithm has input wavelengths different from OLI's center wavelengths. In particular, there is relatively large offset between OLI's λ_4 band (655 nm) and QAA's red band (670 nm). To reduce the uncertainty due to the band mismatch, we converted the input $R_{rs}(\lambda_4)$ to $R_{rs}(670)$ by a polynomial equation ($R^2=0.99$),

$$R_{rs}(670)=10^{P_1X^3+P_2X^2+P_3X+P_4}, \tag{7}$$

with X the log10-transformed original input $R_{rs}(\lambda_4)$ and the model coefficients $P_1=0.0775$, $P_2=0.6585$, $P_3=2.7692$, and $P_4=1.433$. This step is essential for the accurate determination of the total absorption coefficient from QAA when the reference wavelength is set to 670 nm.

QAA first converts the $R_{rs}(\lambda_{0\text{-}4})$ spectra to the subsurface remote sensing reflectance (r_{rs}) following Lee et al. (2002),

$$r_{rs}(\lambda)=\frac{R_{rs}(\lambda)}{0.52+1.7R_{rs}(\lambda)}. \tag{8}$$

Based on numerical simulations of the radiative transfer equations, Gordon et al. (1988) indicated that r_{rs} is a function of the bulk absorption coefficient (a) and the total backscattering coefficient (b_b),

$$r_{rs}(\lambda)=g_0\frac{b_b(\lambda)}{a(\lambda)+b_b(\lambda)}+g_1\left[\frac{b_b(\lambda)}{a(\lambda)+b_b(\lambda)}\right]^2, \tag{9}$$

where g_0 and g_1 are determined to be 0.089 and 0.125 sr^{-1}, respectively (Lee et al., 2002). From the above quadratic equation, $u=b_b/(a+b_b)$ can be solved as a function of r_{rs}, g_0, and g_1.

QAA then proceeds with the estimation of the bulk absorption coefficient at a reference wavelength a (λ_{ref}) with $\lambda_{\text{ref}}=561$ nm if $R_{rs}(670)<0.0015$ sr^{-1}. Otherwise, a (λ_{ref}) will be derived at $\lambda_{\text{ref}}=670$ nm. With estimated a (λ_{ref}), the backscattering coefficient at λ_{ref} can be readily derived as below:

$$b_{bp}(\lambda_{ref})=\frac{u(\lambda_{ref})\times a(\lambda_{ref})}{1-u(\lambda_{ref})}-b_{bw}(\lambda_{ref}), \tag{10}$$

where b_{bp} is the particle backscattering coefficient and b_{bw} is the backscattering coefficient of pure seawater spectrally weighted by OLI's RSR function (Lee et al., 2016). From b_{bp} (λ_{ref}), the spectral backscattering coefficient at bands $\lambda_{0\text{-}4}$ can be derived from the power law model (Gordon & Morel, 1983),

$$b_{bp}(\lambda_i) = b_{bp}(\lambda_{ref})\left(\frac{\lambda_{ref}}{\lambda_i}\right)^{\eta}, i = 0, 1, 2, 3 \text{ and } 4, \tag{11}$$

where η can be estimated empirically from the reflectance at 443 and 561 nm (Lee et al., 2016). The spectral absorption coefficient is then derived as

$$a(\lambda_i) = (1-u(\lambda_i))\left(b_{bw}(\lambda_i) + b_{bp}(\lambda_i)\right)/u(\lambda_i). \tag{12}$$

The QAA algorithm treats the absorption coefficients of CDOM and detritus together, which is analytically solved as below (Lee et al., 2002):

$$a_{dg}(443) = \frac{[a(412)-\zeta a(443)]-[a_w(412)-\zeta a_w(443)]}{\xi-\zeta}. \tag{13}$$

The parameter ζ is estimated as an inverse function of $r_{rs}(443)/r_{rs}(561)$, while ξ is equal to $\exp[S_{dg}\times(443-412)]$, which is further modeled as an inverse function of $r_{rs}(443)/r_{rs}(561)$. With determined $a_{dg}(443)$, the phytoplankton absorption coefficient can be readily derived as the difference between $a(443)$ and $a_{dg}(443)$, after accounting for pure seawater's contribution,

$$a_{ph}(443) = a(443)-a_{dg}(443)-a_w(443). \tag{14}$$

To further partition $a_{dg}(443)$ into dissolved and detrital components, we estimated the absorption coefficient of detritus with the algorithm developed by Dong et al. (2013),

$$a_d(443) = 0.6\times\sigma^{0.9}, \tag{15}$$

where σ is parameterized as

$$\sigma = 0.05\times a_{pg}(443) + b_{bp}(561)\times 1.4^{\frac{R_{rs}(561)+R_{rs}(670)}{R_{rs}(443)}}. \tag{16}$$

This model takes into account the nonwater absorption (a_{pg}) as well as the backscattering of the particles. The spectral absorption coefficient of a_d is then quantified as

$$a_d(\lambda) = a_d(443)\exp[-S_d(\lambda-443)], \tag{17}$$

where the spectral slope S_d was assumed to be a constant, $S_d \approx 0.012$ nm^{-1} (Babin et al., 2003). Finally, the absorption coefficient of CDOM was derived as the difference between $a_{dg}(\lambda)$ and $a_d(\lambda)$.

The procedures and components of SAVE are schematically shown in a flowchart in Figure 2. The configuration allows for further tuning of the LUT, the virtual-band estimator, and the IOP inversion algorithms whenever necessary in the future.

3. Data and Analysis

3.1. Data Acquisition

We used two independent data sets to assess the accuracy of the SAVE algorithm: the NASA bio-Optical Marine Algorithm Data (NOMAD) (Werdell & Bailey, 2005) and the in situ hyperspectral data retrieved from the SeaWiFS Bio-optical Archive and Storage System (SeaBASS; Hooker et al., 1994). With respect to each data set, we performed the following data reduction.

The NOMAD database consists of multiband spectra for R_{rs}, a_{ph}, a_{dg}, a_g, a_d, and b_{bp} centered at 405, 411, 443, 455, 465, 489, 510, 520, 530, 550, 555, 560, 565, 570, 590, 619, 625, 665, 670, and 683 nm. Yet it is noteworthy that many R_{rs} and IOP values are missing, probably a result of the multiband instruments used. To create sufficient and utilizable data for the evaluation in this context, we extended the multiband a_d and a_g measurements over a total of 61 spectral bands evenly distributed between 400 and 700 nm following an exponential-decay model as equation (17), with measured $a_d(443)$ and $a_g(443)$ and corresponding spectral slope data (S_d and S_g). Similarly, we interpolated linearly the phytoplankton absorption spectra to the

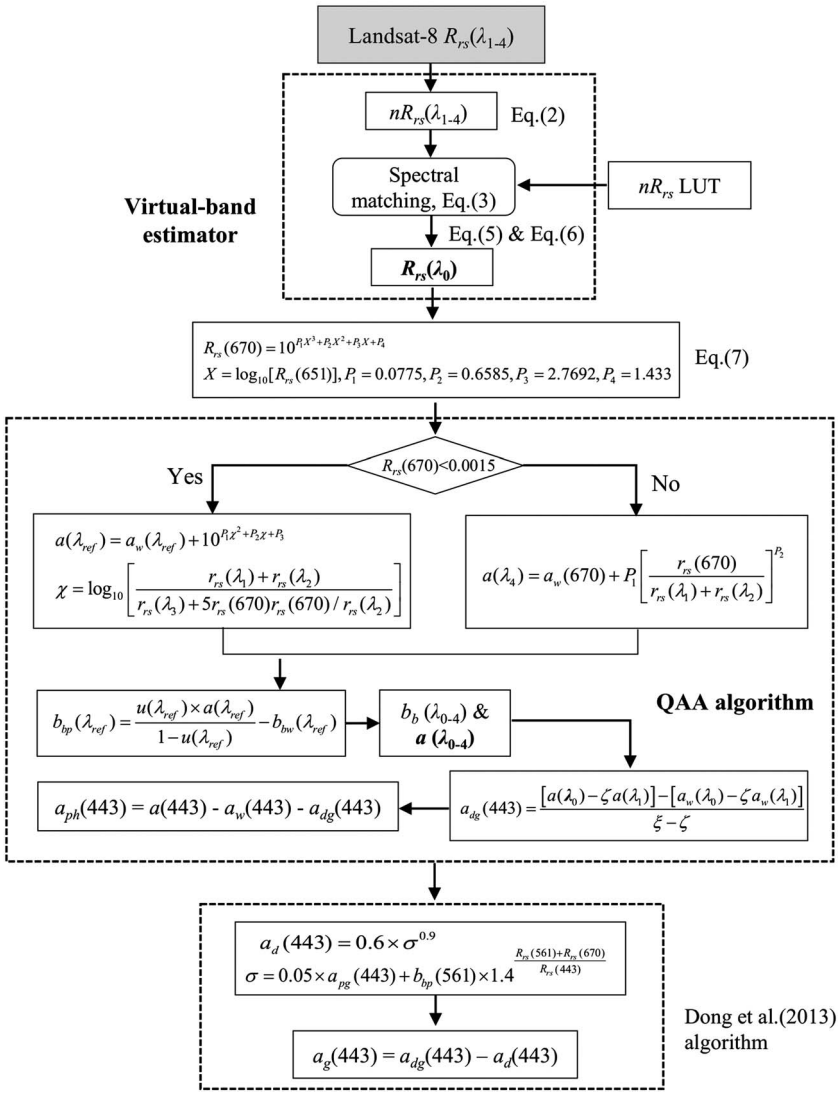

Figure 2. Flowchart for the Semi-Analytical algorithm with a Virtual-band Estimator algorithm to estimate phytoplankton, colored dissolved organic matter, and detritus absorption coefficients from Landsat 8/OLI $R_{rs}(\lambda_{1\text{-}4})$ spectra.

same 61 spectral bands. The hyperspectral b_{bp} data were obtained by the power law model of equation (11), based on the measured $b_{bp}(555)$, with the parameter η estimated as $\eta = \log_{10}[b_{bp}(443)/b_{bp}(510)]/\log_{10}[510/443]$. Quality control was further performed to make sure that only the data with $0 < \eta < 2.5$ were kept for subsequent application. With these hyperspectral IOP spectra, we employed Hydrolight to simulate the R_{rs} spectra. We assumed the same air-water boundary condition, scattering phase function for particles, inelastic scattering, and water depths with the simulations in section 2.1. We only considered a clear sky with the solar zenith angle at 30°. As a result, we obtained 454 hyperspectral R_{rs} spectra for the given IOP data.

The SeaBASS database archives a large amount of R_{rs} measurements with IOP data. For the present analyses, we extracted the hyperspectral data from selected nearshore waters including Boston Harbor and Massachusetts Bay (2017-2018), the Great Lakes (2013-2014), Chesapeake Bay (2011), and the northern Gulf of Mexico (2013). The majority of the R_{rs} spectra were measured by the HyperPro radiometers floating at the water surface with a skylight-blocking approach (137 bands, 350-800; Lee et al., 2013) or profiling of the upper water columns (Mueller et al., 2003). In Chesapeake Bay, the radiometric data were measured with a hand-held radiometer and postprocessed using the method of Lee et al. (2010). The CDOM

samples were collected through 0.2-μm filters, and the CDOM absorption coefficient was measured by the scanning spectrophotometers (250-800 nm). Samples for particulate absorption were captured using 25 mm precombusted GF/F filters (pore size 0.7 μm), and the absorption coefficient of particles (a_p) was determined using the quantitative filter pad technique (QFT; Mitchell et al., 2002). The particles-loaded filter was later bleached using methanol to remove phytoplankton pigments to determine the absorption coefficient by nonalgae particles. The phytoplankton absorption coefficient was then derived as the difference between a_p and a_d ($a_{ph} = a_p - a_d$).

The hyperspectral R_{rs} and backscattering data were convolved to OLI's bands at $\lambda_{1\text{-}4}$ according to equation (1). The absorption coefficient is inversely proportional to reflectance and was derived following Lee et al. (2016),

$$a_x(\lambda_i) = \frac{\int_{400}^{800} RSR^i d\lambda}{\int_{400}^{800} [1/a_x(\lambda)] RSR^i d\lambda}, \mathrm{i} = 1, 2, 3, \text{and } 4, \tag{18}$$

where a_x refers to a_{ph}, a_{pg}, a_g, or a_d. At $\lambda_0 = 412$ nm, the corresponding R_{rs} values were interpolated from the hyperspectral data, without spectral convolution.

3.2. Validation Analyses

To quantify the accuracy of model-estimated quantities, the median absolute percentage difference (MAPD) was derived as

$$MAPD = median\left\{\left|\left(M_j - T_j\right)/T_j\right| \times 100\%\right\}, \tag{19}$$

where M_j and T_j refer to the estimated and known values under investigation, respectively, and j varies from 1 to n, the total number of valid observation involved in the evaluation. The signed relative difference or error (δ) was calculated for the model-estimated $R_{rs}(412)$ values, as the following:

$$\delta = \left(M_j - T_j\right)/T_j \times 100\%. \tag{20}$$

Besides, the root mean square difference (RMSD) was analyzed for each estimated and known quantities, defined as

$$RMSD = \left[\frac{1}{n-1}\sum_{j=1}^{n}\left[M_j - T_j\right]^2\right]^{1/2}. \tag{21}$$

We also performed the model II regression analyses of the log10-transformed quantities and computed the slope and the coefficient of determination (R^2). Nonrealistic retrievals such as the negative values due to imperfect model architectures were excluded from the statistical analysis. As a result, the number of valid retrievals involved in the validation analyses, n, can sometimes be less than the total number of input R_{rs} spectra, N.

3.3. Sensitivity Analyses

To understand how the uncertainty of the estimated $R_{rs}(412)$ impacts the retrieved absorption coefficients, we carried out the following sensitivity analyses. The IOCCG synthetic data (IOCCG, 2006), considered free of measurement uncertainty, were used. The data ($N = 500$) were divided into three subgroups with respect to their chlorophyll concentrations: the eutrophic (CHL $\geq$ 1 mg/m^3), mesotrophic (0.1 $\leq$ CHL $<$ 1 mg/m^3), and oligotrophic waters (CHL $<$ 0.1 mg/m^3). We convolved the R_{rs} and IOP spectra of each subgroup to Landsat 8/OLI bands and interpolated them to λ_0. Assuming the "error-free" $R_{rs}(\lambda_{1\text{-}4})$ spectra, we disturbed the $R_{rs}(412)$ values with random errors,

$$R_{rs}^{err}(412) = R_{rs}(412) + \mathfrak{R}\cdot\delta, \tag{22}$$

where $R_{rs}^{err}(412)$ represents the error-disturbed values, $\mathfrak{R}$ is a random number between 0 and 1 of standard normal distribution, and δ is the relative difference of $R_{rs}(412)$ to its true value. Nine instances of δ were

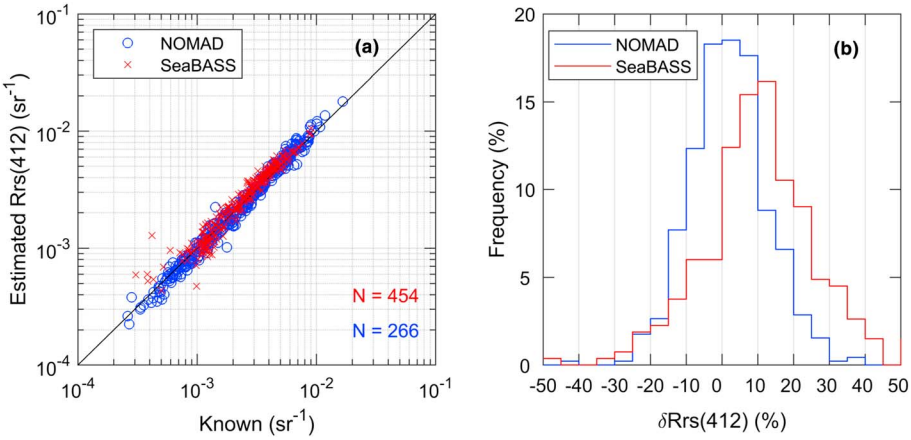

Figure 3. (a) Comparison of estimated $R_{rs}(412)$ by the Semi-Analytical algorithm with a Virtual-band Estimator algorithm with known $R_{rs}(412)$ for NASA bio-Optical Marine Algorithm Data (NOMAD) data and SeaWiFS Bio-optical Archive and Storage System (SeaBASS) data, with the accompanying regression statistics given in Table 1; (b) frequency distribution of the relative difference of modeled $R_{rs}(412)$ with respect to known values for the synthetic data (in blue) and in situ data (in red).

considered, which vary from −20%, −15%, −10%, −5%, 0%, +5%, +10%, +15%, and finally to +20%. The SAVE algorithm was implemented directly with these erroneous R_{rs} spectra following the workflow starting with equation (7) (Figure 2), that is, revoking the virtual-band estimator. The median of the unbiased percentage difference (denoted as Δ) was calculated between the model-estimated absorption coefficients from the erroneous R_{rs} spectra and those from error-free R_{rs} spectra, that is, $\delta R_{rs}(412) = 0$, as

$$\Delta = median\left\{2\times\left|\frac{E_j - F_j}{E_j + F_j}\right|\times 100\%\right\}, j = 1, 2, ..., n, \tag{23}$$

where E_j refers to the model retrievals with the error-disturbed R_{rs} spectra, while F_j is the corresponding optical properties inverted from the error-free R_{rs} spectra. In the following, we treat Δ as the uncertainty of the model-estimated absorption coefficients originated from $\delta R_{rs}(412)$.

4. Results

4.1. Evaluation of $R_{rs}(412)$ Retrievals

As $R_{rs}(412)$ is critical for the proposed algorithm, we first evaluate the accuracy for the estimated $R_{rs}(412)$ values (see Figure 3a and Table 1). For the NOMAD data, the estimated $R_{rs}(412)$ are reasonably consistent with known values with small differences (MAPD = 7% and RMSD = 0.00044 sr^{-1}). The SeaBASS data span a relatively narrower dynamic range, with $R_{rs}(412)$ varying between 0.001 and 0.009 sr^{-1}; the estimated $R_{rs}(412)$ data are overall consistent with the measured values of SeaBASS data (MAPD = 11% and RMSD = 0.00045 sr^{-1}). In addition, regression analyses between the estimated and known $R_{rs}(412)$ values obtained linear slopes only slightly deviated from unity (1.05 and 1.04 for NOMAD and SeaBASS data, respectively). Furthermore, we compared the frequency distribution of the relative errors of the estimated $R_{rs}(412)$ (Figure 3b). It is found that the relative errors ($\delta R_{rs}(412)$) are positively skewed. The NOMAD estimation has the first mode at 2%, while the SeaBASS estimation shows a larger first mode at around 12%. This discrepancy can be partly attributable to the uncertainty or errors of the in situ R_{rs} measurements and partly to the uncertainty of the algorithm itself. In spite of the biases, more than 90% of the estimated $R_{rs}(412)$ are found subjected to a relatively small error with $\delta R_{rs}(412)$ varying between −20% and 20% for the SeaBASS data. A few outliers are present with the estimated SeaBASS $R_{rs}(412)$ (Figure 3a), which contribute to the positive tail of the frequency distribution (Figure 3b). These outliers represent highly absorptive waters, with $R_{rs}(412) < 0.001$ sr^{-1}. The measurement uncertainties of these R_{rs} spectra are partly responsible for the discrepancy between estimated and known $R_{rs}(412)$ values.

Table 1
Regression Statistics and Validation Results of SAVE Estimations for NOMAD (N = 454) and SeaBASS (N = 266) Data

		NOMAD data (N = 454)					SeaBASS data (N = 266)				
		n	Slope	R^2	MAPD	RMSDa	n	Slope	R^2	MAPD	RMSD
R_{rs}	412	454	1.05	0.99	7%	0.00044	266	1.04	0.94	11%	0.00045
a	412	454	0.92	0.97	19%	0.27	266	1.01	0.90	17%	0.4
	443	454	0.90	0.97	18%	0.2	266	0.95	0.86	19%	0.36
a_{ph}	412	442	0.90	0.76	33%	0.13	255	0.97	0.68	38%	0.19
	443	454	0.92	0.77	30%	0.14	266	0.97	0.65	39%	0.22
a_{dg}	412	454	0.97	0.93	28%	0.28	266	0.97	0.86	25%	0.44
	443	454	0.97	0.92	30%	0.18	266	0.97	0.78	32%	0.34
a_g	412	454	0.97	0.87	35%	0.28	265	0.97	0.77	37%	0.45
	443	454	0.97	0.86	35%	0.15	266	0.97	0.64	46%	0.33
a_d	412	454	0.97	0.81	67%	0.21	266	0.97	0.86	57%	0.28
	443	454	0.97	0.80	67%	0.16	266	0.97	0.86	56%	0.21

Note. SAVE = SemiAnalytical algorithm with a Virtual-band Estimator; NOMAD = NASA bio-Optical Marine Algorithm Data; SeasBASS = SeaWiFS Bio-optical Archive and Storage System; MAPD = median absolute percentage difference; RMSD = root mean square difference. Note that the regression statistics was performed with log-transformed data. *N* is the number of R_{rs} data tested, and *n* is the number of valid model retrievals.
[a]The unit is sr^{-1} for R_{rs} data and m^{-1} for absorption coefficient.

The variation of $\delta R_{rs}(412)$ was further assessed with respect to the chlorophyll concentrations (Figure 4a). Interestingly, there is a slightly negative trend between $\delta R_{rs}(412)$ and CHL. The $\delta R_{rs}(412)$ slowly vary from positive to negative when CHL increases from <0.1 to >10 mg/m^3. On the other hand, a weak but positive trend exists between $\delta R_{rs}(412)$ and $R_{rs}(412)$ (Figure 4b). The dependencies of $\delta R_{rs}(412)$ on CHL and $R_{rs}(412)$ are not contradictive, as smaller $R_{rs}(412)$ values are often suggestive of stronger phytoplankton and CDOM absorption, and vice versa. According to the illustrations in Figure 4, the $\delta R_{rs}(412)$ can be relatively larger in very low-CHL waters or very high-CHL waters. For the former case, the $R_{rs}(412)$ values are high, but the $R_{rs}(\lambda_{1\text{-}4})$ spectra usually vary over a narrow range, which may impact the spectral-shape-based classification as equation (3). For the latter case, the $R_{rs}(412)$ values can be very small, leading to larger percentage differences.

Overall, the differences between the estimated and known $R_{rs}(412)$ values are small. According to the validation analyses, the satellite-derived $R_{rs}(412)$ are often subject to an MAPD of greater than 20% from their in situ matchups in nearshore environments (Qin et al., 2017; Zibordi et al., 2009). In addition, the in situ measurements of $R_{rs}(412)$ from different measurement platforms can differ from each other with MAPD > ~10% (Hooker et al., 2002). So we can conclude that the above-discussed small differences for the estimated $R_{rs}(412)$ provide a confident measure of the virtual-band estimator in these waters.

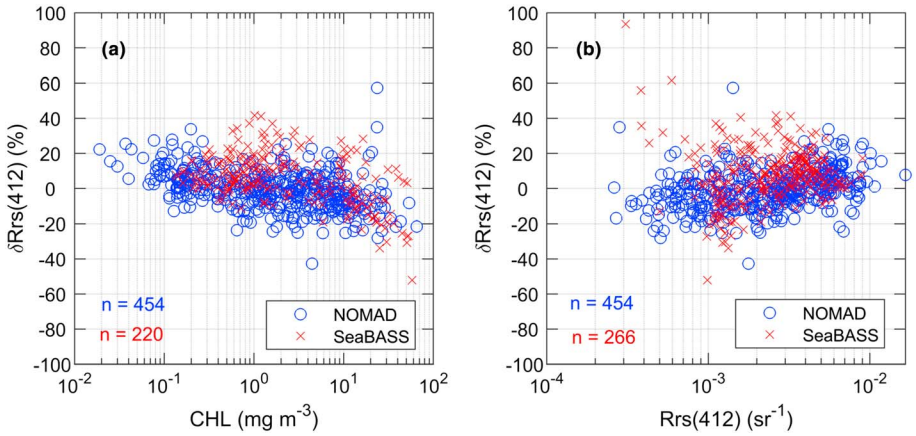

Figure 4. Variation of $\delta R_{rs}(412)$ with water trophic status (panel a) and the magnitudes of $R_{rs}(412)$ (panel b) for NASA bio-Optical Marine Algorithm Data (NOMAD; denoted by open circles) and SeaWiFS Bio-optical Archive and Storage System (SeaBASS) data (denoted by crosses). The legends are the same as Figure 3a. Note that the number of in situ data used in (a) and (b) is different due to data availability.

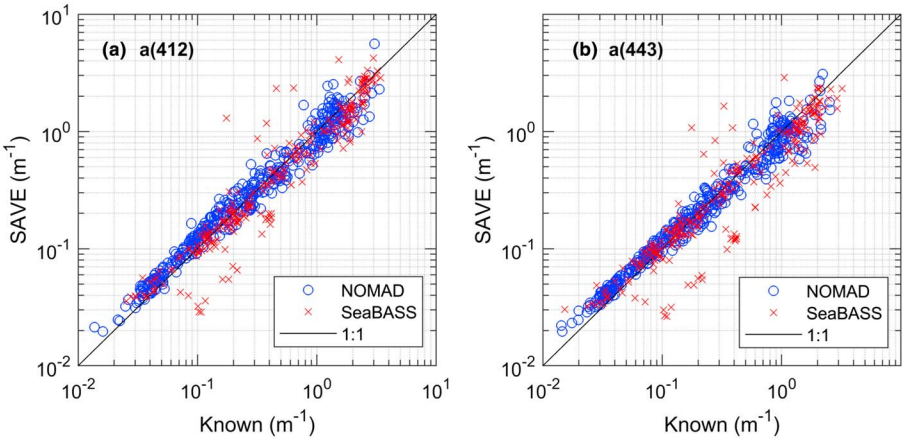

Figure 5. Comparison of Semi-Analytical algorithm with a Virtual-band Estimator (SAVE)-estimated total absorption coefficients with known values for NASA bio-Optical Marine Algorithm Data (NOMAD; denote as open circles) and SeaWiFS Bio-optical Archive and Storage System (SeaBASS) data (denoted as crosses). The regression and validation statistics is given in Table 1.

4.2. Evaluation of Bulk, Phytoplankton, and CDM Absorption Coefficient Retrievals

The model-estimated bulk absorption coefficients at 412 and 443 nm are favorably comparable to known values (Figure 5 and Table 1). First, we stress that the retrieval of $a(443)$ is irrelevant to the estimation of $R_{rs}(412)$ under the framework of QAA. Rather, $a(443)$ is solely determined by $R_{rs}(\lambda_{1\text{-}4})$. For NOMAD, the $a(412)$ and $a(443)$ retrievals agree well (MAPD = 16-17%, RMSD = 0.22-0.2 m^{-1}, and $R^2 = 0.97$) with known values over the full dynamic range of the test data (0.02-3 m^{-1}). The retrievals of $a(412)$ and $a(443)$ for SeaBASS are slightly less accurate (MAPD = 17-19%, RMSD = 0.36-0.4 m^{-1}, and $R^2 = 0.86$-0.9), a result of the uncertainties from both R_{rs} and IOP measurements. The retrievals for the component absorption coefficients a_{ph} and a_{dg} suffer larger uncertainties than the total absorption coefficients (Table 1 and Figure 6). This is related to the step-by-step nature of ocean color inversion as implemented by QAA where R_{rs} is governed by the bulk optical properties, not individual components. Therefore more uncertainties or errors are expected in the retrieved component absorption coefficients $a_{ph}(443)$ and $a_{dg}(443)$ when they are partitioned from $a(412)$ and $a(443)$ (Figure 2). The uncertainties in $a(412)$ and $a(443)$ propagate to and impact the estimated $a_{ph}(443)$ and $a_{dg}(443)$ (Lee et al., 2010). Considering the error metrics and regression analyses, the agreement between retrieved and known a_{dg} values at two blue bands is better than a_{ph}. The differential performance for a_{dg} and a_{ph} estimation is common with the SA algorithms (IOCCG, 2006; Werdell et al., 2013) and can be partly explained by the fact that a_{dg} dominates the total absorption coefficients at two blue bands for the majority (>80%) of the NOMAD and SeaBASS data used herein. In addition, it is also likely related to the difficulty in modeling the spectral shapes for phytoplankton absorption, which vary significantly in natural waters (Bricaud et al., 2004; Roesler et al., 1989). Some outliers are present with the SeaBASS a_{dg} retrievals, which are most probably a result of the problems with sampling of inhomogeneous waters (IOCCG, 2018). The uncertainties induced by these outliers further propagated to the total absorption coefficients and affected their comparison (Figure 5). In comparison, the retrievals for SeaBASS data have shown larger variability (with higher RMSD) than those for NOMAD data. This is partly related to the fact that we simulated the R_{rs} spectra for the NOMAD data, which are free of measurement uncertainty.

The performance of our approach in estimating $a(412)$ is comparable to other SA algorithms, which used the $R_{rs}(412)$ measurements for the inversion (e.g., Loisel et al., 2018; Werdell et al., 2013). The MAPD values varying between 30% and 39% (see Table 1) are not a small uncertainty for $a_{ph}(443)$ and $a_{dg}(443)$ estimation. But it is not uncommon to observe such evaluation results for ocean color inversion algorithms, since the in situ data and the SA algorithms are always subject to uncertainties. For comparison, Werdell et al. (2013) showed that the estimated NOMAD $a_{ph}(443)$ and $a_{dg}(443)$ from the generalized IOP (GIOP) algorithm have an uncertainty with MAPD equal to 26% and 35%, respectively; their results compare favorably to ours (30% and 30% for $a_{ph}(443)$ and $a_{dg}(443)$, respectively). Note that they used more data points from the NOMAD data set ($n = 682$) than the present study ($n = 454$) but the absorption coefficients span approximately the

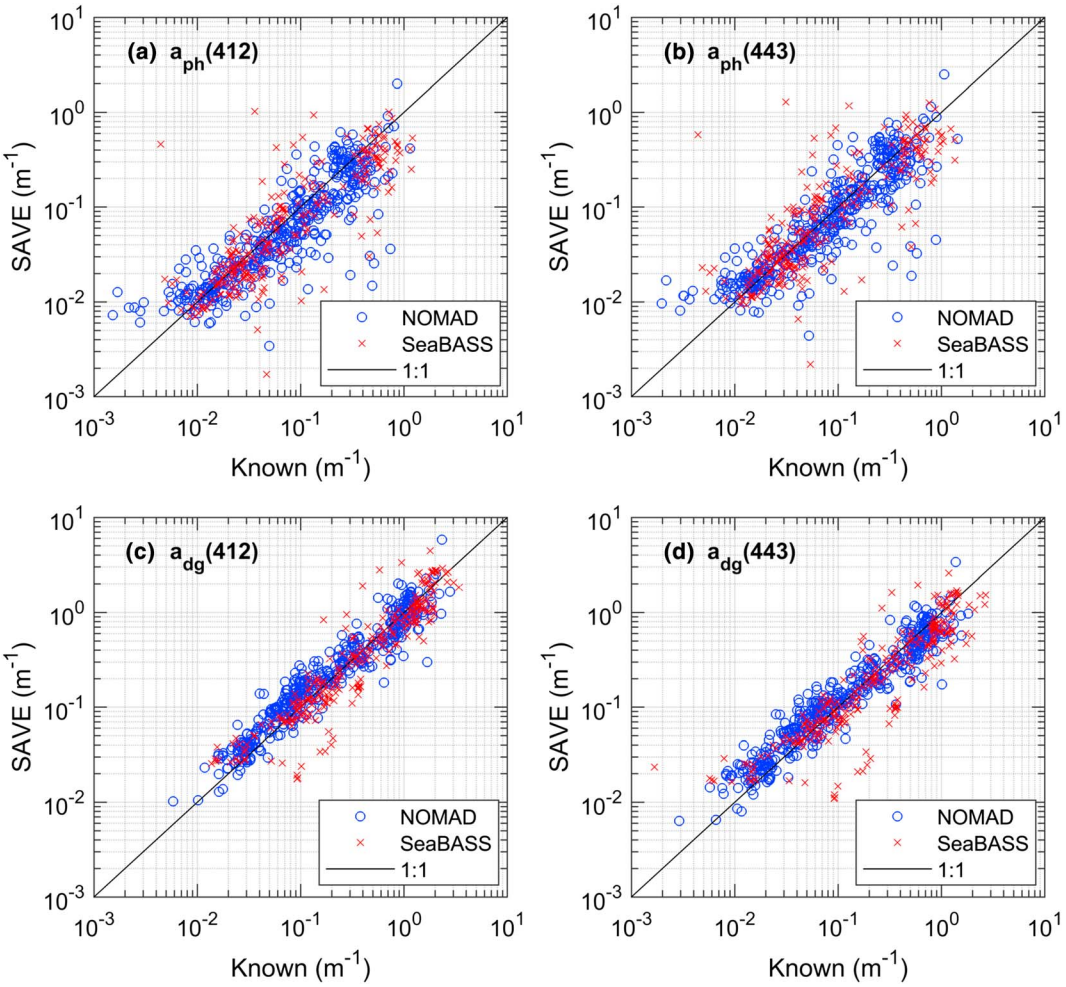

Figure 6. Comparison of Semi-Analytical algorithm with a Virtual-band Estimator (SAVE)-estimated a_{ph} and a_{dg} with known values for the NASA bio-Optical Marine Algorithm Data (NOMAD; denote by open circles) and SeaWiFS Bio-optical Archive and Storage System (SeaBASS) data (denoted by crosses). The regression and validation statistics is given in Table 1.

same dynamic range as the present analyses. Smyth et al. (2006) analyzed their SA algorithm with NOMAD data ($n = 459$) and reported for the absorption retrievals less accurate than the results shown here, which is partly related to the narrower dynamic range of the data used therein. From the above analyses, we can reach a conclusion that our approach can generate retrievals for the bulk, phytoplankton, and CDM absorption coefficients from Landsat 8/OLI reflectance, with accuracy comparable to previous analyses.

4.3. Evaluation of CDOM and Detritus Absorption Coefficient Retrievals

It is important to reiterate that the SA algorithms generally do not partition the absorption coefficients of CDOM and detritus because of their similar spectral behaviors (Lee et al., 2002; Maritorena et al., 2002; Smyth et al., 2006; Werdell et al., 2013). The procedure adopted herein for the estimation of detritus absorption a_d is empirical in nature. It suffers the uncertainties from the estimation of a(443) and b_{bp}(561) but is irrelevant to R_{rs}(412). As the intermediate product, the a_d retrievals at 412 and 443 nm are subject to large MAPD varying between 56% and 67%, in spite of the high R^2 and close-to-one slopes (Figure 7 and Table 1). The a_d(412) and a_d(443) retrievals tend to be overestimated for $a_d < 0.01$ m^{-1} and underestimated for $a_d > 0.1$ m^{-1}. The negative bias is particularly significant for the NOMAD data when $a_d > 0.1$ m^{-1}. This may be caused by the measurement uncertainty of the particle absorption coefficients (IOCCG, 2018; Neeley et al., 2015). In contrast, the retrieval of the CDOM absorption coefficient a_g relies on the

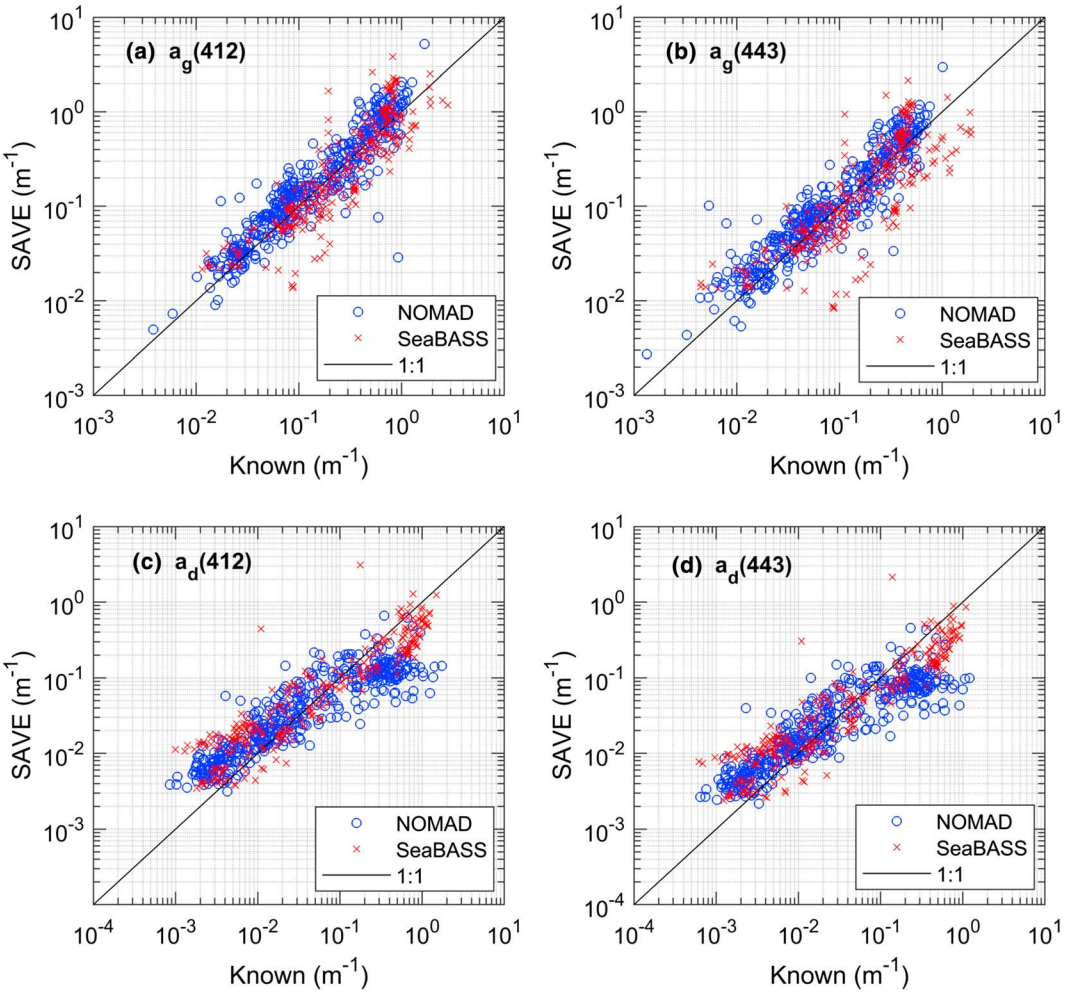

Figure 7. Comparison of Semi-Analytical algorithm with a Virtual-band Estimator (SAVE)-estimated a_g and a_d with known values for NASA bio-Optical Marine Algorithm Data (NOMAD; denote by open circles) and SeaWiFS Bio-optical Archive and Storage System (SeaBASS) data (denoted by crosses). The regression and validation statistics is given in Table 1.

knowledge of $R_{rs}(412)$, which allows for the derivation of a_{dg} under the framework of QAA. The estimated $a_g(443)$ are much more accurate than $a_d(443)$. This is mostly because the values of $a_d(443)$ are smaller than $a_g(443)$ for the majority of the NOMAD data (>90%) and SeaBASS data (>70%). Our comparison indicates that the accuracy of $a_g(412)$ retrievals are higher than or at least equivalent to $a_g(443)$. This is valuable as the CDOM absorption is strongly correlated with the dissolved organic carbon and salinity in coastal waters (Del Castillo & Miller, 2008; Pan & Wong, 2015; Vantrepotte et al., 2015). Undoubtedly, the SA derivation of $a_g(412)$ (and likely $a_g(443)$) with the present approach will provide support to the study of the carbon stocks and material transport in nearshore environments.

4.4. Sensitivity of Absorption Retrievals to $R_{rs}(412)$ Estimation

The sensitivity of the absorption coefficient retrievals to the relative error of $R_{rs}(412)$ ($\delta R_{rs}(412)$) is summarized in Table 2. Because the estimation of $a(443)$ from QAA does not rely on $R_{rs}(412)$, the uncertainty for $a(443)$ retrieval ($\Delta a(443)$) is independent of $\delta R_{rs}(412)$. As anticipated, however, the uncertainties of other absorption coefficient retrievals do vary with $\delta R_{rs}(412)$. The $a(412)$ values are estimated from $R_{rs}(412)$ and $b_{bp}(412)$; the latter is irrelevant to the estimation of $R_{rs}(412)$ but determined by the $R_{rs}(443)/R_{rs}(561)$ ratios (refer to the QAA algorith; Lee et al., 2002). So it is straightforward to understand that $\Delta a(412)$ increases

Table 2
The Uncertainty Δ (×100) of SAVE-Estimated Absorption Coefficients

Oligotrophic waters ($N = 75$)									
δR_{rs}	412	−20%	−15%	−10%	−5%	5%	10%	15%	20%
Δa	412	18	8	5	3	3	5	9	12
	443	0	0	0	0	0	0	0	0
Δa_{ph}	412	50	27	20	12	14	22	28	34
	443	50	27	20	12	14	22	28	34
Δa_{dg}	412	44	21	14	9	9	16	24	35
	443	44	21	14	9	9	16	24	35
Δa_g	412	48	27	19	12	12	19	31	45
	443	50	28	20	13	12	20	31	46
Mesotrophic waters ($N = 150$)									
δR_{rs}	412	−20%	−15%	−10%	−5%	5%	10%	15%	20%
Δa	412	14	10	6	3	4	6	11	15
	443	0	0	0	0	0	0	0	0
Δa_{ph}	412	44	34	26	13	17	28	43	47
	443	44	34	26	13	17	28	43	47
Δa_{dg}	412	34	24	13	6	9	15	25	36
	443	34	24	13	6	9	15	25	36
Δa_g	412	41	28	16	7	10	18	31	42
	443	42	29	16	8	11	18	32	43
Eutrophic waters ($N = 275$)									
δR_{rs}	412	−20%	−15%	−10%	−5%	5%	10%	15%	20%
Δa	412	15	9	7	3	3	7	9	14
	443	0	0	0	0	0	0	0	0
Δa_{ph}	412	49	35	29	16	15	28	35	47
	443	49	35	29	16	15	28	35	47
Δa_{dg}	412	33	21	15	8	7	16	22	32
	443	33	21	15	8	7	16	22	32
Δa_g	412	46	28	22	11	10	22	31	45
	443	48	29	24	11	10	23	33	48

Note. SAVE = Semi-Analytical algorithm with a Virtual-band Estimator.

with increasing $\delta R_{rs}(412)$. Because we have assumed that $R_{rs}(443)$ and $R_{rs}(561)$ are error free in our analysis, the rate of change in $\Delta a(412)$ is found weak, with resultant $\Delta a(412)$ values smaller than the absolute amplitudes of $\delta R_{rs}(412)$. The uncertainties of the component absorption coefficients are much more sensitive to $\delta R_{rs}(412)$, where Δa_{ph} and Δa_g can be twice larger than the absolute magnitudes of $\delta R_{rs}(412)$. In the mesotrophic waters, for instance, $\Delta a_{ph}(412)$ and $\Delta a_{ph}(443)$ increase from ~27% to ~45% when $\delta R_{rs}(412)$ varies from ±10% to ±20%. This result can be explained by the involvement of $a(412)$ in the separation of $a_{ph}(443)$ and $a_{dg}(443)$, which plays a major role in $\Delta a_{ph}(412)$ and $\Delta a_{ph}(443)$ in QAA (Lee, Arnone, et al., 2010). Among all component absorptions, Δa_{dg} remains least sensitive to $\delta R_{rs}(412)$. In all three types of waters, Δa_{dg} and Δa_g are found roughly comparable to each other. Our analyses only indicate a weak dependence of Δa_{ph} and Δa_{dg} on the chlorophyll a concentrations. Specifically, $\Delta a_{ph}(412)$ and $\Delta a_{ph}(443)$ remain the smallest in the oligotrophic waters, while $\Delta a_{dg}(412)$ and $\Delta a_{dg}(443)$ are the smallest for the eutrophic and mesotrophic waters. For CDOM, we found the smallest Δa_g in the mesotrophic waters. Unlike all above component absorption coefficients, Δa_d does not change with $\delta R_{rs}(412)$, because its derivation is not related to $R_{rs}(412)$ in the present configuration (recalling equations (15) and (16)).

5. Discussion

The Landsat 8/OLI instrument has the potential for generating high-spatial-resolution bio-optical properties in the dynamic nearshore waters. Compared with the operational satellite sensors such as Moderate Resolution Imaging Spectroradiometer and Visible and Infrared Spectroradiometer, Landsat 8/OLI is still short-handed because of the relatively fewer number of visible bands ($\lambda_{1\text{-}4}$ = 443, 482, 561, and 655 nm). Particularly, the lack of a blue band at 412 nm has made it difficult to implement the existing SA algorithms (IOCCG, 2006; Lee et al., 2002; Maritorena et al., 2002; Smyth et al., 2006; Werdell et al., 2013) for the retrieval of component absorption coefficients. The SAVE algorithm is designed to fill this gap. It predicts R_{rs} in a virtual band centered at λ_0 = 412 nm for each individual $R_{rs}(\lambda_{1\text{-}4})$ spectrum. The estimated $R_{rs}(\lambda_0)$ and existing $R_{rs}(\lambda_{1\text{-}4})$ together allow for analytical derivation of absorption coefficients of the major components. This convenient approach makes it practical for generating the absorption coefficients for phytoplankton, CDOM, and detritus from the Landsat 8/OLI data while following the framework of the existing SA algorithms.

The virtual-band estimator is a novel and critical component of the SAVE algorithm. In spite of the encouraging performance, the model still faces challenges. First, the virtual-band estimator evokes spectral matching (or optical classification) based on four-band R_{rs} spectra (recall equation (3)). With too few bands, this matching can introduce uncertainty or error, albeit small. Second, it is impossible for the lookup table to include every R_{rs} spectral shapes existing in natural waters. When the actual R_{rs} shape deviates from the LUT, the matching and subsequent estimation of $R_{rs}(412)$ may suffer sometimes large uncertainty or error. Nevertheless, the analyses suggest that the SAVE algorithm provides a satisfactory estimation for $R_{rs}(412)$ over the high dynamic range of waters with $R_{rs}(412)$ varying between ~0.001 and 0.025 sr^{-1}.

The study here used the NOMAD and SeaBASS data, which are not free of measurement uncertainty. The uncertainty for the particulate absorption coefficient measurements can sometimes be very large (Neeley et al., 2015). The in situ R_{rs} measurements are also subject to uncertainties originating from the calibration, environmental disturbance, postprocessing, and so forth (Wei et al., 2014; Zibordi et al., 2012). Although

difficult to determine, these measurement uncertainties have certainty affected the validation results. According to the sensitivity analyses (Table 2), the influence of the erroneous $R_{rs}(412)$ input data is indeed not negligible under the extreme conditions when $\delta R_{rs}(412)$ approach $\pm 20\%$. The assumption of $\pm 20\%$ errors for $R_{rs}(412)$ is not randomly chosen but inferred from the evaluations of the in situ measurements (Figure 3). We did not further change $\delta R_{rs}(412)$, positively or negatively, because the resultant R_{rs} spectral shapes could be dramatically distorted so that the resultant R_{rs} spectra become unrealistic. A complete understanding of the model uncertainty will demand an investigation of the uncertainty propagation with globally representative data.

As our analyses demonstrated, SAVE provides a feasible avenue for the analytical retrieval of the water component absorption coefficients, particularly for phytoplankton, CDM, and CDOM from the Landsat 8/OLI reflectance data for global applications (Tables 1 and 2). The success of the model benefits from the use of existing SA algorithm, specifically, of QAA (Lee et al., 2002). It is interesting to note the model configuration also allows utilizing the other SA algorithms for optical inversion. For example, one may replace QAA with the spectral-optimization algorithm of GIOP (Werdell et al., 2013) for the purpose of the IOP inversion. Being a temporary solution, the current modeling framework does not rule out the necessity of continuous development of the SA schemes to further improve the model performance for the derivation of light absorption coefficients.

To demonstrate the application of the SAVE algorithm for the monitoring of nearshore waters, we derived the absorption coefficient products from a Landsat 8/OLI image. The Landsat 8/OLI image was captured on 28 August 2015 over Boston Harbor and Massachusetts Bay (Figure 8). The OLI bands 5 and 7 (865 and 2201 nm, respectively) were used for the atmospheric correction and the satellite retrievals flagged as ATMFAIL, LAND, CLDICE, and HILT were masked out. The validation of Landsat 8/OLI R_{rs} spectra with in situ matchups were provided elsewhere (Wei et al., 2018). As shown in Figure 8a, the transport pattern of surface water including the water plumes, bright/dark waterfronts, and ship wakes are captured in the composited true color image. The spatial gradients and distribution patterns of the absorption coefficients for CDM, phytoplankton, and CDOM from the Harbor toward the Bay are clearly shown up in Figures 8b–8d. Within the spatial domain under investigation, the CDOM and the detritus dominate the light absorption coefficients instead of phytoplankton. Also, $a_{ph}(443)$, $a_{dg}(443)$, and $a_g(443)$ are found extremely high near the shorelines and river mouths with values greater than 10 m^{-1} for Landsat 8/OLI measurements of this time. The absorption products in the strongly absorptive waters with $a > 1$ m^{-1} have not been fully validated though due to lack of concurrent field measurements. As suggested in Figures 8b–8d, there exists significant difference in the distribution patterns of $a_{ph}(443)$ and $a_{dg}(443)$ (and $a_g(443)$) products). Such difference is attributable to the fact that the phytoplankton does not covary with CDM, CDOM, or detritus, a phenomenon commonly occurring in optically complex nearshore waters. The decoupling of $a_{ph}(443)$ and $a_{dg}(443)$ is of significant implication for the estimation of phytoplankton biomass in such aquatic environments. In water color remote sensing, the empirical blue-green spectral band ratios of R_{rs} spectra such as $R_{rs}(482)/R_{rs}(561)$ are often used for CHL retrievals (Franz et al., 2015; Snyder et al., 2017). The band-ratio algorithms are sensitive to the bulk absorption and work relatively well for "case 1" water (Gregg & Casey, 2004; Moore et al., 2009). But the reflectance ratios become less sensitive to the changes of CHL as the CDOM and/or detritus absorption starts to play increasingly important roles in the bulk absorption (Dierssen, 2010). As a result, the comparison of the CHL retrieval from the band-ratio algorithm (Figure 8e) with the $a_{ph}(443)$ retrieval can show strikingly different spatial distribution patterns. For these particular observations, the spatial distribution of the CHL product is much more similar to $a_{dg}(443)$ and $a_g(443)$, indicating erroneous CHL product for such nearshore waters when it is estimated using blue-green band-ratio algorithms. The SA retrieval of $a_{ph}(443)$ from the current approach likely provides more accurate estimation for the autotrophic biomass with fine details.

The framework of SAVE is designed with the objective to facilitate the use of the Landsat 8/OLI reflectance data. It is certainly feasible to implement it with reflectance measurements from other radiometers as long as they share similar band settings with the OLI sensor. For instance, the Sentinel 2 satellite is equipped with the MultiSpectral Instrument (MSI). The MSI has four visible bands centered at 444, 497, 560, and 664 nm, almost identical to Landsat 8/OLI. The future Landsat 9 satellite will have the OLI-2. The algorithm developed in this study should be readily applicable to MSI and OLI-2 imageries.

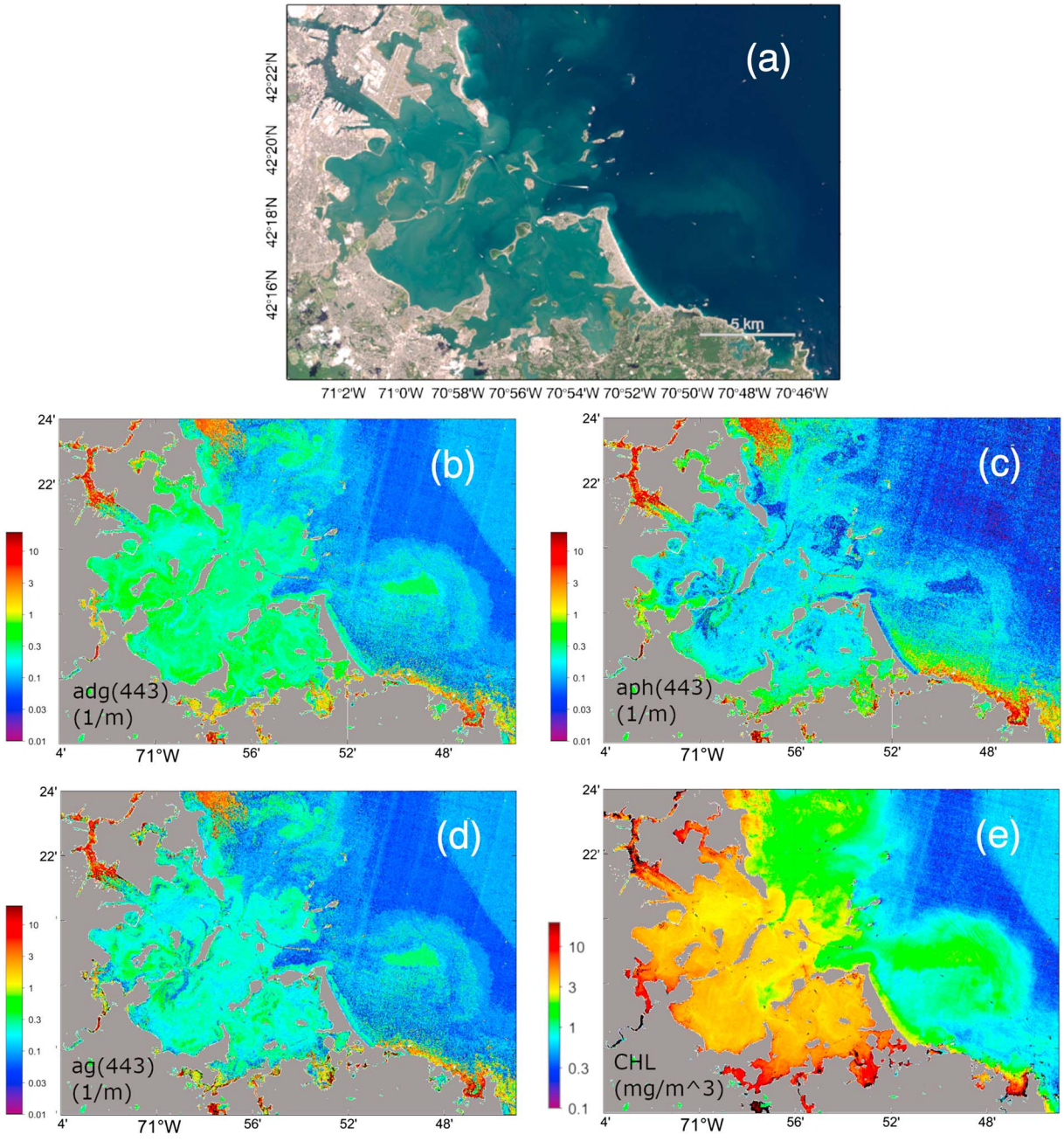

Figure 8. Landsat 8/Operational Land Imager true color image (LC80120312015240) of Boston Harbor and Massachusetts Bay (panel a) and mapping products of retrieved component absorption coefficients $a_{ph}(443)$, $a_{dg}(443)$, and $a_g(443)$ (unit: per meter) from Semi-Analytical algorithm with a Virtual-band Estimator (panels b–d). Panel (e) is the chlorophyll a concentrations (unit: milligram per cubic meter) derived from the fourth-order polynomial function of $R_{rs}(482)/R_{rs}(561)$ ratios with coefficients determined by NASA.

6. Concluding Remarks

Landsat 8/OLI is an advanced multiband and high-resolution satellite sensor and can generate high-quality reflectance product for the coastal waters. Since its launch in 2013, the Landsat 8 data have been widely used in water-related studies on a variety of topics. Partly due to the lack of a 412-nm band, however, it remains challenging to apply existing SA algorithms to Landsat 8/OLI reflectance product for derivation of the light absorption coefficients for various water components. Consequently, the Landsat 8 data have not received sufficient attention in wider applications to coastal water remote sensing as it should have deserved after

6-year operation. In this study, we developed SAVE to facilitate the derivation of phytoplankton, CDOM, and detritus absorption coefficients from the Landsat 8/OLI reflectance. SAVE employs a virtual-band estimator to estimate R_{rs} at 412 nm from the existing reflectance spectra measured at other bands. It is found that such estimated $R_{rs}(412)$ is acceptably accurate over the full dynamic range of the test data, with MAPD of 7% and 11% for the NOMAD and SeaBASS data, respectively. Thus, the estimation of $R_{rs}(412)$ allows to use existing SA inversion algorithms for derivation of the component absorption coefficients of waters. In current analysis, we adopted the QAA to derive $a_{ph}(443)$ and $a_{dg}(443)$. The $a_{ph}(443)$ retrievals are found only subject to an uncertainty with MAPD = 30% and MAPD = 39% for NOMAD and SeaBASS data, respectively. The estimated $a_{dg}(443)$ suffer an uncertainty with MAPD = 30% for NOMAD and MAPD = 32% for SeaBASS data. These uncertainty statistics are comparable with those of existing SA algorithms using the $R_{rs}(412)$ measurements. The SAVE algorithm further partitions a_{dg} into a_g and a_d with an existing algorithm of Dong et al. (2013). The accuracy of the estimated a_g (MAPD = 35–47%) is found comparable with a_{ph} retrievals. Our analyses suggest that it is feasible to use the new approach to semianalytically generate the component absorption coefficients for the global waters with $a(443)$ varying between 0.01 and 3 m^{-1}, with acceptable accuracy. The semianalytically derived phytoplankton absorption coefficient is arguably a more reliable proxy for phytoplankton biomass in coastal waters where the phytoplankton is often decoupled with CDOM and detritus. On the other hand, the CDOM and detritus absorption coefficients will also provide important information for aquatic biology, carbon cycles, and other climate-related problems.

Acknowledgments
This study was supported by the NASA projects (NNX15AC84G, NNX16AD38G, and 80NSSC18K0509), the NOAA VIIRS Cal/Val project (NA11OAR4320199), and the Natural Science Foundation of China (NSFC) (No.41576169). We thank the NASA OBPG for distributing the NOMAD and SeaBASS data and the principal investigators for contributing data to SeaBASS. Thanks also go to two anonymous reviewers for comments and recommendation. The MATLAB script is developed for the current algorithm and accessible online (http://oceanoptics.umb.edu/resources/). Data are available from authors.

References

Alcântara, E., Watanabe, F., Rodrigues, T., & Bernardo, N. (2016). An investigation into the phytoplankton package effect on the chlorophyll-a specific absorption coefficient in Barra Bonita reservoir, Brazil. *Remote Sensing Letters*, *7*(8), 761–770. https://doi.org/10.1080/2150704X.2016.1185189

Babin, M., Stramski, D., Ferrari, G. M., Claustre, H., Bricaud, A., Obolensky, G., & Hoepffner, N. (2003). Variations in the light absorption coefficients of phytoplankton, nonalgal particles, and dissolved organic matter in coastal waters around Europe. *Journal of Geophysical Research, Oceans*, *108*(4), 3211. https://doi.org/10.1029/2001JC000882

Binding, C. E., Jerome, J. H., Bukata, R. P., & Booty, W. G. (2008). Spectral absorption properties of dissolved and particulate matter in Lake Erie. *Remote Sensing of Environment*, *112*(4), 1702–1711. https://doi.org/10.1016/j.rse.2007.08.017

Brando, V. E., Dekker, A. G., Park, Y. J., & Schroeder, T. (2012). Adaptive semianalytical inversion of ocean color radiometry in optically complex waters. *Applied Optics*, *51*(15), 2808–2833. https://doi.org/10.1364/AO.51.002808

Bricaud, A., Claustre, H., Ras, J., & Oubelkheir, K. (2004). Natural variability of phytoplanktonic absorption in oceanic waters: Influence of the size structure of algal populations. *Journal of Geophysical Research*, *109*, C11010. https://doi.org/10.1029/2004JC002419

Bricaud, A., Morel, A., & Prieur, L. (1981). Absorption by dissolved organic matter of the sea (yellow substance) in the UV and visible domains. *Limnology and Oceanography*, *26*(1), 43–53. https://doi.org/10.4319/lo.1981.26.1.0043

Cao, F., & Miller, W. L. (2015). A new algorithm to retrieve chromophoric dissolved organic matter (CDOM) absorption spectra in the UV from ocean color. *Journal of Geophysical Research: Oceans*, *120*, 496–516. https://doi.org/10.1002/2014JC010241

Carder, K. L., Chen, F. R., Lee, Z. P., Hawes, S. K., & Kamykowski, D. (1999). Semianalytic Moderate-resolution Imaging Spectrometer algorithms for chlorophyll-a and absorption with bio-optical domains based on nitrate-depletion temperatures. *Journal of Geophysical Research*, *104*(C3), 5403–5421. https://doi.org/10.1029/1998JC900082

Carder, K. L., Hawes, S. K., Baker, K. A., Smith, R. C., Steward, R. G., & Mitchell, B. G. (1991). Reflectance model for quantifying chlorophyll a in the presence of productivity degradation products. *Journal of Geophysical Research*, *96*(C11), 20,599–20,611. https://doi.org/10.1029/91JC02117

Ciotti, A. M., & Bricaud, A. (2006). Retrievals of a size parameter for phytoplankton and spectral light absorption by colored detrital matter from water-leaving radiances at SeaWiFS channels in a continental shelf region off Brazil. *Limnology and Oceanography: Methods*, *4*(7), 237–253. https://doi.org/10.4319/lom.2006.4.237

Del Castillo, C. E., & Miller, R. L. (2008). On the use of ocean color remote sensing to measure the transport of dissolved organic carbon by the Mississippi River Plume. *Remote Sensing of Environment*, *112*(3), 836–844. https://doi.org/10.1016/j.rse.2007.06.015

Dierssen, H. M. (2010). Perspectives on empirical approaches for ocean color remote sensing of chlorophyll in a changing climate. *Proceedings of the National Academy of Sciences of the United States of America*, *107*(40), 17,073–17,078. https://doi.org/10.1073/pnas.0913800107

Dong, Q., Shang, S., & Lee, Z. P. (2013). An algorithm to retrieve absorption coefficient of chromophoric dissolved organic matter from ocean color. *Remote Sensing of Environment*, *128*, 259–267. https://doi.org/10.1016/j.rse.2012.10.013

Franz, B. A., Bailey, S. W., Kuring, N., & Werdell, P. J. (2015). Ocean color measurements with the Operational Land Imager on Landsat-8: implementation and evaluation in SeaDAS. *Journal of Applied Remote Sensing*, *9*(1), 096070–096070. https://doi.org/10.1117/1.JRS.9.096070

Gordon, H. R., Brown, O. B., Evans, R. H., Brown, J. W., Smith, R. C., Baker, K. S., & Clark, D. K. (1988). A semianalytic radiance model of ocean color. *Journal of Geophysical Research*, *93*(D9), 10,909–10,924. https://doi.org/10.1029/JD093iD09p10909

Gordon, H. R., & Morel, A. (1983). *Remote assessment of ocean color for interpretation of satellite visible imagery: A review*, (p. 44). New York: Springer-Verlag. https://doi.org/10.1029/LN004

Gregg, W. W., & Casey, N. W. (2004). Global and regional evaluation of the SeaWiFS chlorophyll data set. *Remote Sensing of Environment*, *93*(4), 463–479. https://doi.org/10.1016/j.rse.2003.12.012

Hansell, D. A., & Carlson, C. A. (2001). Marine dissolved organic matter and the carbon cycle. *Oceanography*, *14*(4), 41–49. https://doi.org/10.5670/oceanog.2001.05

Hoge, F. E., & Lyon, P. E. (1996). Satellite retrieval of inherent optical properties by linear matrix inversion of oceanic radiance models: an analysis of model and radiance measurement errors. *Journal of Geophysical Research*, *101*(C7), 16,631–16,648. https://doi.org/10.1029/96JC01414

Hooker, S. B., Lazin, G., Zibordi, G., & McLean, S. (2002). An evaluation of above- and in-water methods for determining water-leaving radiances. *Journal of Atmospheric and Oceanic Technology*, *19*(4), 486–515. https://doi.org/10.1175/1520-0426(2002)019<0486:AEOAAI>2.0.CO;2

Hooker, S. B., McClain, C. R., Firestone, J. K., Westphal, T. L., Yeh, E.-N., & Ge, Y. (1994). The SeaWiFS bio-optical archive and storage system (SeaBASS), Part 1*Rep*., 1-40 pp, , Greenbelt, Maryland: NASA Goddard Space Flight Center.

IOCCG (2006). Remote sensing of inherent optical properties: Fundamentals, tests of algorithms, and applications, *International Ocean-Colour Coordinating Group Rep. 5*, 126 pp, Dartmouth, Nova Scotia, Canada: International Ocean Color Coordinating Group.

IOCCG (2018). Inherent optical property measurements and protocols: Absorption coefficient. In A. Neeley & A. Mannino (Eds.), *IOCCG ocean optics and biogeochemistry protocols for satellite ocean color sensor validation* (p. 78). Dartmouth, Canada: International Ocean Color Coordinating Group (IOCCG). https://doi.org.10.25607/OBP-119

Kim, W., Moon, J.-E., Park, Y.-J., & Ishizaka, J. (2016). Evaluation of chlorophyll retrievals from Geostationary Ocean Color Imager (GOCI) for the North-East Asian region. *Remote Sensing of Environment*, *184*, 482–495. https://doi.org/10.1016/j.rse.2016.07.031

Lee, Z. P., Ahn, Y.-H., Mobley, C., & Arnone, R. (2010). Removal of surface-reflected light for the measurement of remote-sensing reflectance from an above-surface platform. *Optics Express*, *18*(25), 26,313–26,324. https://doi.org/10.1364/OE.18.026313

Lee, Z. P., Arnone, R., Hu, C., Werdell, P. J., & Lubac, B. (2010). Uncertainties of optical parameters and their propagations in an analytical ocean color inversion algorithm. *Applied Optics*, *49*(3), 369–381. https://doi.org/10.1364/AO.49.000369

Lee, Z. P., Carder, K. L., & Arnone, R. (2002). Deriving inherent optical properties from water color: a multi-band quasi-analytical algorithm for optically deep waters. *Applied Optics*, *41*(27), 5755–5772. https://doi.org/10.1364/AO.41.005755

Lee, Z. P., Carder, K. L., Mobley, C. D., Steward, R. G., & Patch, J. S. (1998). Hyperspectral remote sensing for shallow waters. 1. A semi-analytical model. *Applied Optics*, *37*(27), 6329–6338. https://doi.org/10.1364/AO.37.006329

Lee, Z. P., Pahlevan, N., Ahn, Y.-H., Greb, S., & O'Donnell, D. (2013). Robust approach to directly measuring water-leaving radiance in the field. *Applied Optics*, *52*(8), 1693–1701. https://doi.org/10.1364/AO.52.001693

Lee, Z. P., Shang, S., Qi, L., Yan, J., & Lin, G. (2016). A semi-analytical scheme to estimate Secchi-disk depth from Landsat-8 measurements. *Remote Sensing of Environment*, *177*, 101–106. https://doi.org/10.1016/j.rse.2016.02.033

Lee, Z. P., Wei, J., Shang, Z., Garcia, R., Dierssen, H. M., Ishizaka, J., & Castagna, A. (2019). On-water radiometry measurements: Skylight-blocked approach and data processing*Rep*., Dartmouth, Nova Scotia, Canada: IOCCG.

Lee, Z. P., Wei, J., Voss, K., Lewis, M., Bricaud, A., & Huot, Y. (2015). Hyperspectral absorption coefficient of "pure" seawater in the range of 350-550 nm inverted from remote sensing reflectance. *Applied Optics*, *54*(3), 546–558. https://doi.org/10.1364/AO.54.000546

Loisel, H., Stramski, D., Dessailly, D., Jamet, C., Li, L., & Reynolds, R. A. (2018). An inverse model for estimating the optical absorption and backscattering coefficients of seawater from remote-sensing reflectance over a broad range of oceanic and coastal marine environments. *Journal of Geophysical Research: Oceans*, *123*, 2141–2171. https://doi.org/10.1002/2017JC013632

Mannino, A., Novak, M. G., Hooker, S. B., Hyde, K., & Aurin, D. (2014). Algorithm development and validation of CDOM properties for esturine and continental shelf waters along the northeastern U.S. coast. *Remote Sensing of Environment*, *152*, 576–602. https://doi.org/10.1016/j.rse.2014.06.027

Maritorena, S., Siegel, D. A., & Peterson, A. R. (2002). Optimization of a semianalytical ocean color model for global-scale applications. *Applied Optics*, *41*(15), 2705–2714. https://doi.org/10.1364/AO.41.002705

Markham, B., Barsi, J., Kvaran, G., Ong, L., Kaita, E., Biggar, S., et al. (2014). Landsat-8 Operational Land Imager radiometric calibration and stability. *Remote Sensing*, *6*(12), 12,275–12,308. https://doi.org/10.3390/rs61212275

Mitchell, B. G., Kahru, M., Wieland, J., & Stramska, M. (2002). Determination of spectral absorption coefficients of particles, dissolved material and phytoplankton for discrete water samples. In J. L. Mueller & G. S. Fargion (Eds.), *Above-water radiance and remote sensing reflectance measurement and analysis protocols* (pp. 231–257). Maryland: NASA, NASA Goddard Space Flight Center, Greenbelt.

Mobley, C. D. (1994). *Light and water: Radiative transfer in natural waters* (p. 592). San Diego, California: Academic Press.

Mobley, C. D., & Sundman, L. K. (2008). *Hydrolight 5 and Ecolight 5 user's guide*, edited, p, (p. 99). Bellevue, WA: Sequoia Scientific, Inc.

Moore, T. S., Campbell, J. W., & Dowell, M. D. (2009). A class-based approach to characterizing and mapping the uncertainty of the MODIS ocean chlorophyll product. *Remote Sensing of Environment*, *113*(11), 2424–2430. https://doi.org/10.1016/j.rse.2009.07.016

Morel, A. (1991). Light and marine photosynthesis: A spectral model with geochemical and climatological implications. *Progress in Oceanography*, *26*(3), 263–306. https://doi.org/10.1016/0079-6611(91)90004-6

Mueller, J. L., Fargion, G. S., & McClain, C. R. (2003). Radiometric measurements and data analysis protocols, *Ocean Optics Protocols for Satellite Ocean Color Sensor Validation Rep. NASA/TM-2003-21621/Rev-Vol III*, 78 pp, Greenbelt, MD: NASA Goddard Space Flight Center.

Neeley, A. R., Freeman, S. A., & Harris, L. A. (2015). Multi-method approach to quantify uncertainties in the measurements of light absorption by particles. *Optics Express*, *23*(24), 31,043–31,058. https://doi.org/10.1364/OE.23.031043

Olmanson, L. G., Brezonik, P. L., Finlay, J. C., & Bauer, M. E. (2016). Comparison of Landsat 8 and Landsat 7 for regional measurements of CDOM and water clarity in lakes. *Remote Sensing of Environment*, *185*, 119–128. https://doi.org/10.1016/j.rse.2016.01.007

Pahlevan, N., Schott, J. R., Franz, B. A., Zibordi, G., Markham, B., Bailey, S., et al. (2017). Landsat 8 remote sensing reflectance (Rrs) products: Evaluations, intercomparisons, and enhancements. *Remote Sensing of Environment*, *190*, 289–301. https://doi.org/10.1016/j.rse.2016.12.030

Pan, X., & Wong, G. T. F. (2015). An improved algorithm for remotely sensing marine dissolved organic carbon: Climatology in the northern South China Sea shelf-sea and adjacent waters. *Deep-Sea Research. Pt. II*, *117*, 131–142. https://doi.org/10.1016/j.dsr2.2015.02.025

Qin, P., Simis, S. G. H., & Tilstone, G. H. (2017). Radiometric validation of atmospheric correction for MERIS in the Baltic Sea based on continuous observations from ships and AERONET-OC. *Remote Sensing of Environment*, *200*, 263–280. https://doi.org/10.1016/j.rse.2017.08.024

Roesler, C. S., Perry, M. J., & Carder, K. L. (1989). Modeling in situ phytoplankton absorption from total absorption spectra in productive inland marine waters. *Limnology and Oceanography*, *34*(8), 1510–1523. https://doi.org/10.2307/2837036

Siegel, D. A., Maritorena, S., Nelson, N. B., & Behrenfeld, M. J. (2005). Independence and interdependencies among global ocean color properties: Reassessing the bio-optical assumption. *Journal of Geophysical Research*, *110*, C07011. https://doi.org/10.1029/2004JC002527

Smyth, T. J., Moore, G. F., Hirata, T., & Aiken, J. (2006). Semianalytical model for the derivation of ocean color inherent optical properties: Description, implementation, and performance assessment. *Applied Optics*, *45*(31), 8116–8131. https://doi.org/10.1364/AO.45.008116

Snyder, J., Boss, E., Weatherbee, R., Thomas, A. C., Brady, D., & Newell, C. (2017). Oyster aquaculture site selection using Landsat 8-derived sea surface temperature, turbidity, and chlorophyll a. *Frontiers in Marine Science*, *4*(190). https://doi.org/10.3389/fmars.2017.00190

Vantrepotte, V., Danhiez, F.-P., Loisel, H., Ouillon, S., Mériaux, X., Cauvin, A., & Dessailly, D. (2015). CDOM-DOC relationship in contrasted coastal waters: implication for DOC retrieval from ocean color remote sensing observation. *Optics Express*, *23*(1), 33–54. https://doi.org/10.1364/OE.23.000033

Wei, J., Lee, Z. P., Garcia, R., Zoffoli, M. L., Armstrong, R., Shang, Z., et al. (2018). An assessment of Landsat-8 atmospheric correction schemes and remote sensing reflectance products in coral reefs and coastal turbid waters. *Remote Sensing of Environment*, *215*, 18–32. https://doi.org/10.1016/j.rse.2018.05.033

Wei, J., Lee, Z. P., Ondrusek, M., Mannino, A., Tzortziou, M., & Armstrong, R. (2016). Spectral slopes of the absorption coefficient of colored dissolved and detrital material inverted from UV-visible remote sensing reflectance. *Journal of Geophysical Research: Oceans*, *121*, 1953–1969. https://doi.org/10.1002/2015JC011415

Wei, J., Lee, Z. P., & Shang, S. (2016). A system to measure the data quality of spectral remote sensing reflectance of aquatic environments. *Journal of Geophysical Research: Oceans*, *121*, 8189–8207. https://doi.org/10.1002/2016JC012126

Wei, J., Lewis, M. R., Van Dommelen, R., Zappa, C. J., & Twardowski, M. S. (2014). Wave-induced light field fluctuations in measured irradiance depth profiles: A wavelet analysis. *Journal of Geophysical Research: Oceans*, *119*, 1344–1364. https://doi.org/10.1002/2013JC009572

Werdell, P. J., & Bailey, S. W. (2005). An improved bio-optical data set for ocean color algorithm development and satellite data product validation. *Remote Sensing of Environment*, *98*(1), 122–140. https://doi.org/10.1016/j.rse.2005.07.001

Werdell, P. J., Franz, B. A., Bailey, S. W., Feldman, G. C., Boss, E., Brando, V. E., et al. (2013). Generalized ocean color inversion model for retrieving marine inherent optical properties. *Applied Optics*, *52*(10), 2019–2037. https://doi.org/10.1364/AO.52.002019

Werdell, P. J., McKinna, L. I. W., Boss, E., Ackleson, S. G., Craig, S. E., Gregg, W. W., et al. (2018). An overview of approaches and challenges for retrieving marine inherent optical properties from ocean color remote sensing. *Progress in Oceanography*, *160*, 186–212. https://doi.org/10.1016/j.pocean.2018.01.001

Whitmire, A. L., Boss, E., Cowles, T. J., & Pegau, W. S. (2007). Spectral variability of the particulate backscattering ratio. *Optics Express*, *15*(11), 7019–7031. https://doi.org/10.1364/OE.15.007019

Yu, X., Shen, F., & Liu, Y. (2016). Light absorption properties of CDOM in the Changjiang (Yangtze) estuarine and coastal waters: An alternative approach for DOC estimation. *Estuarine, Coastal and Shelf Science*, *181*, 302–311. https://doi.org/10.1016/j.ecss.2016.09.004

Zhang, X., Hu, L., & He, M.-X. (2009). Scattering by pure seawater: Effect of salinity. *Optics Express*, *17*(7), 5698–5710. https://doi.org/10.1364/OE.17.005698

Zibordi, G., Berthon, J.-F., Mélin, F., D'Alimonte, D., & Kaitala, S. (2009). Validation of satellite ocean color primary products at optically complex coastal sites: Northern Adriatic Sea, Northern Baltic Proper and Gulf of Finland. *Remote Sensing of Environment*, *113*(12), 2574–2591. https://doi.org/10.1016/j.rse.2009.07.013

Zibordi, G., Ruddick, K., Ansko, I., Moore, G., Kratzer, S., Icely, J., & Reinart, A. (2012). In situ determination of the remote sensing reflectance: An inter-comparison. *Ocean Science*, *8*(4), 567–586. https://doi.org/10.5194/os-8-567-2012